Electronic Supplementary Material (ESI)

for

The Legacy of AAZTA - Synthesis and Coordination Chemistry of Two AAZTA Structural Analogues

Federico Forgione,[1,2] Madalina Ranga,[3] Fabio Travagin,[1] Mariangela Boccalon,[3] Zsolt Baranyai,[3] Giovanni B. Giovenzana,[1,2] Luciano Lattuada[4,*]

[1] Dipartimento di Scienze del Farmaco (DSF), Università del Piemonte Orientale, Largo Donegani 2, I-28100, Novara, Italy
[2] CAGE Chemicals srl, Via Bovio 6, 28100 Novara (NO), Italy;
[3] Bracco Imaging Spa, CRB Trieste, AREA Science Park, 34149 Basovizza (TS), Italy;
[4] Bracco Imaging SpA, Via Egidio Folli, 20134 Milano, Italy;
* Luciano.Lattuada@bracco.com

Table of contents

NMR spectra

Figure S1. ^{1}H NMR spectrum of compound 2a.
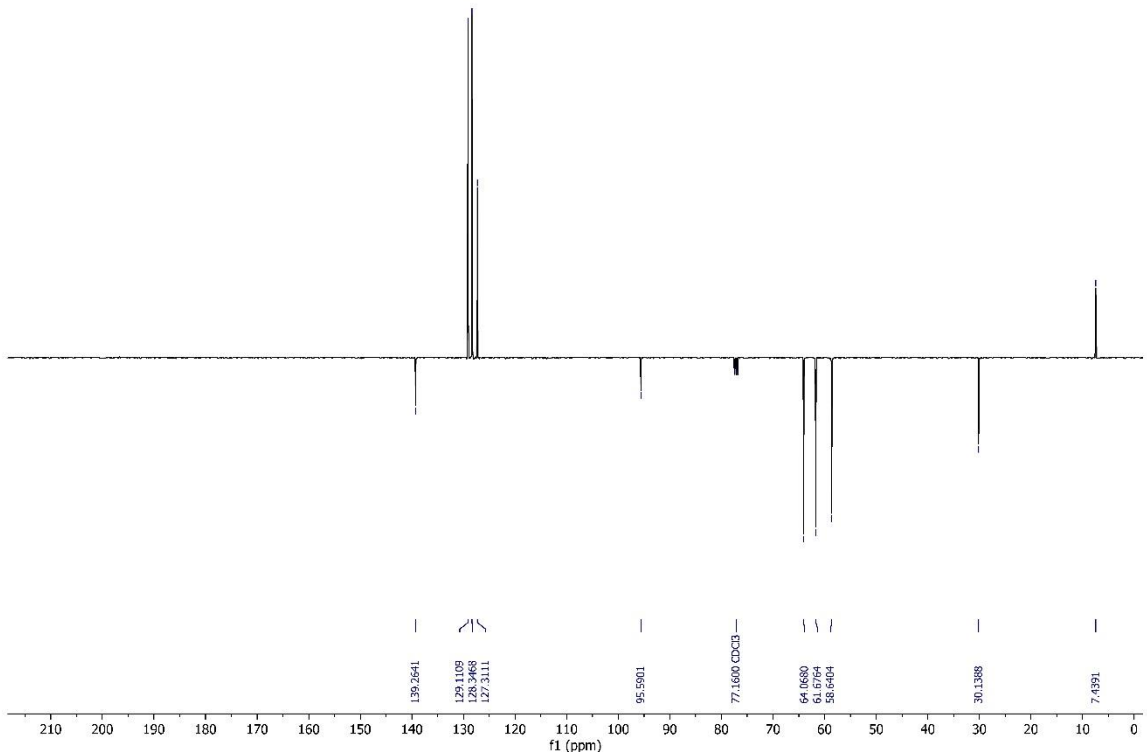
Figure S2. ^{13}C APT NMR spectrum of compound 2a.
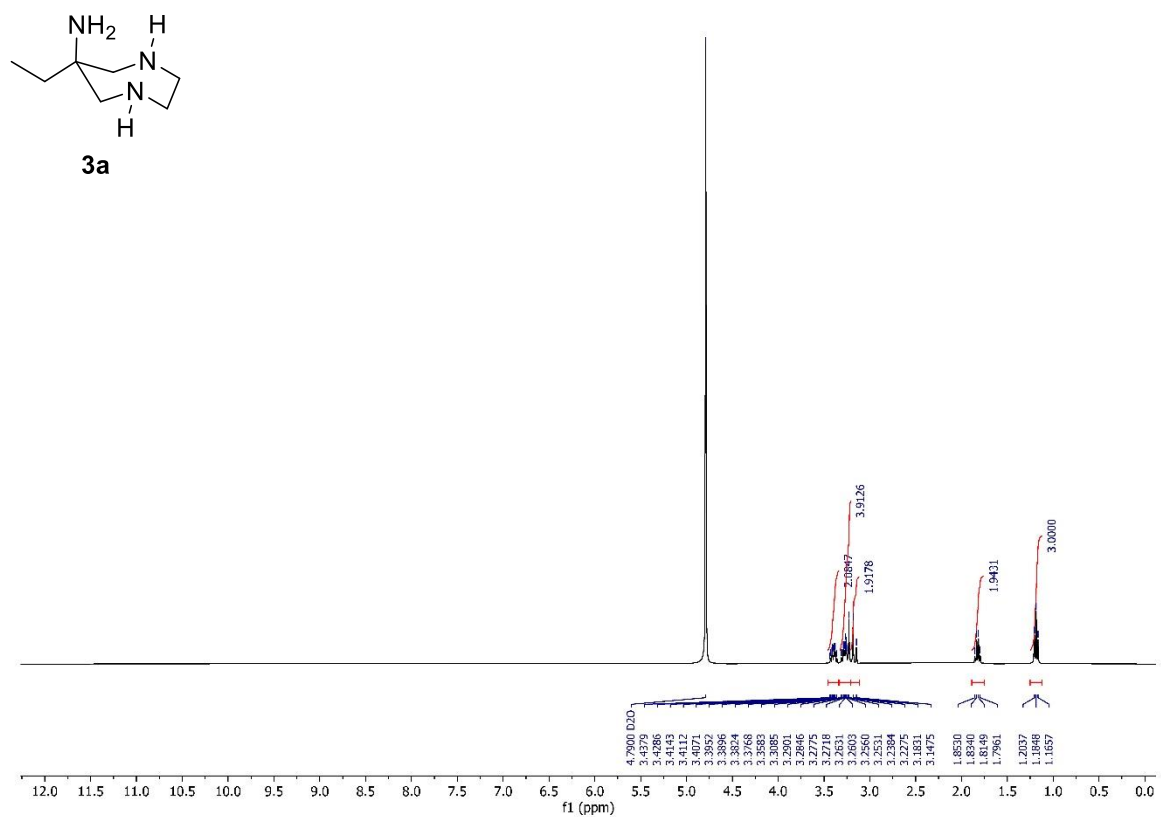
Figure S3. ^{1}H NMR spectrum of compound **3a**.
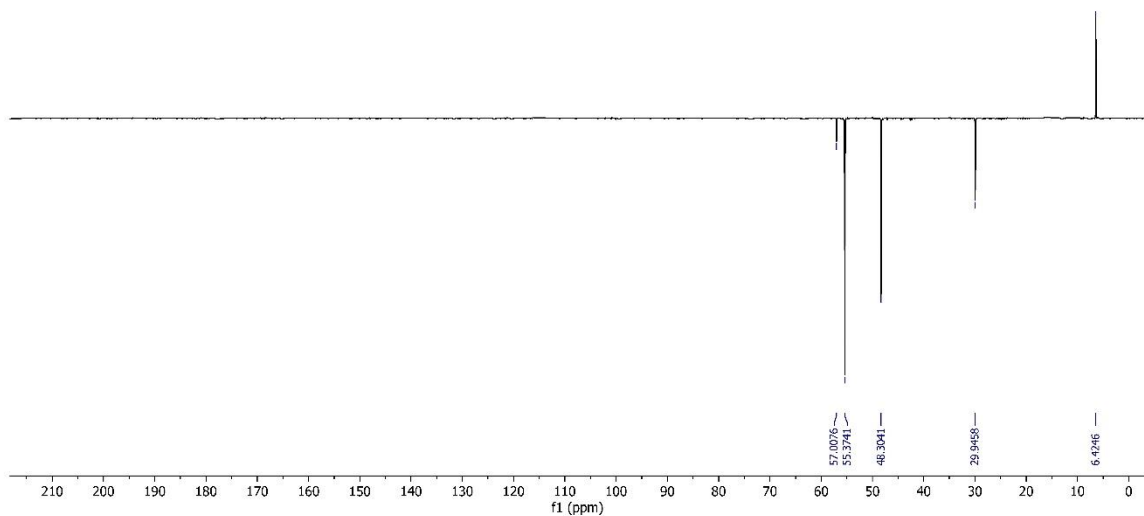
Figure S4. ^{13}C APT NMR spectrum of compound **3a**.
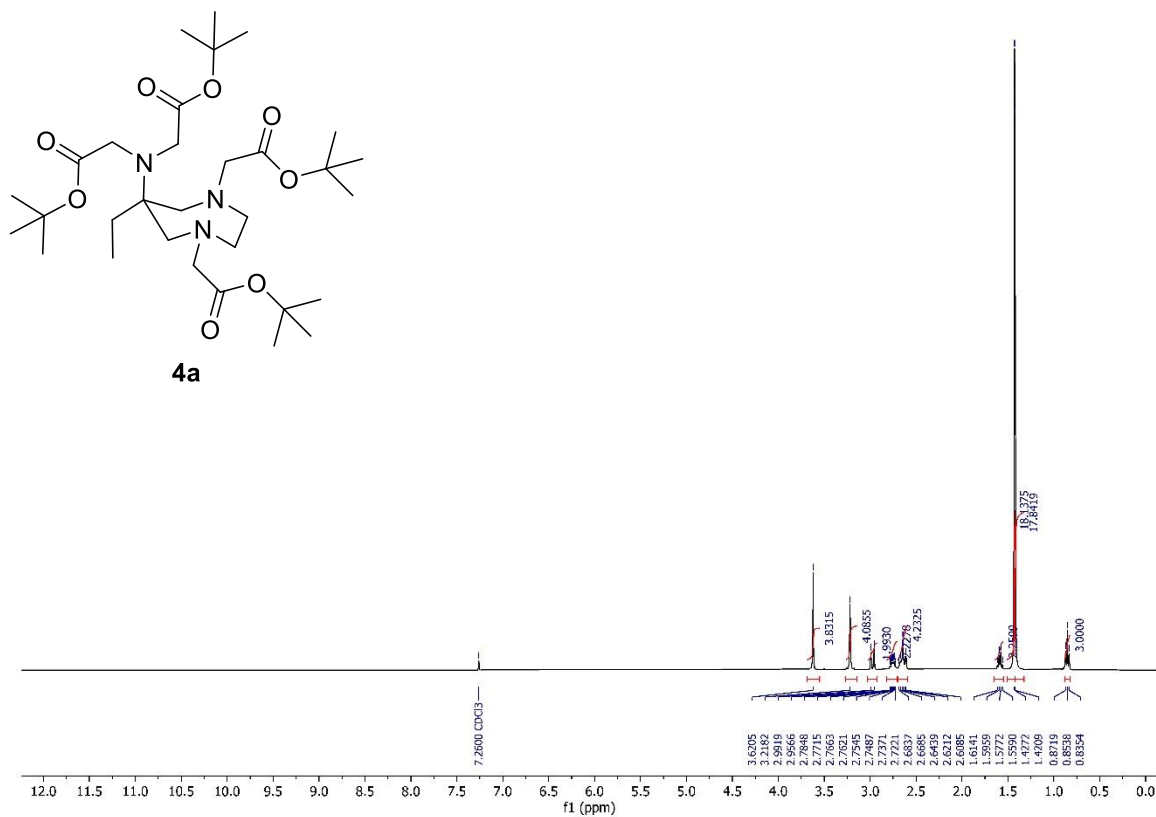
Figure S5. ^{1}H NMR spectrum of compound **4a**.
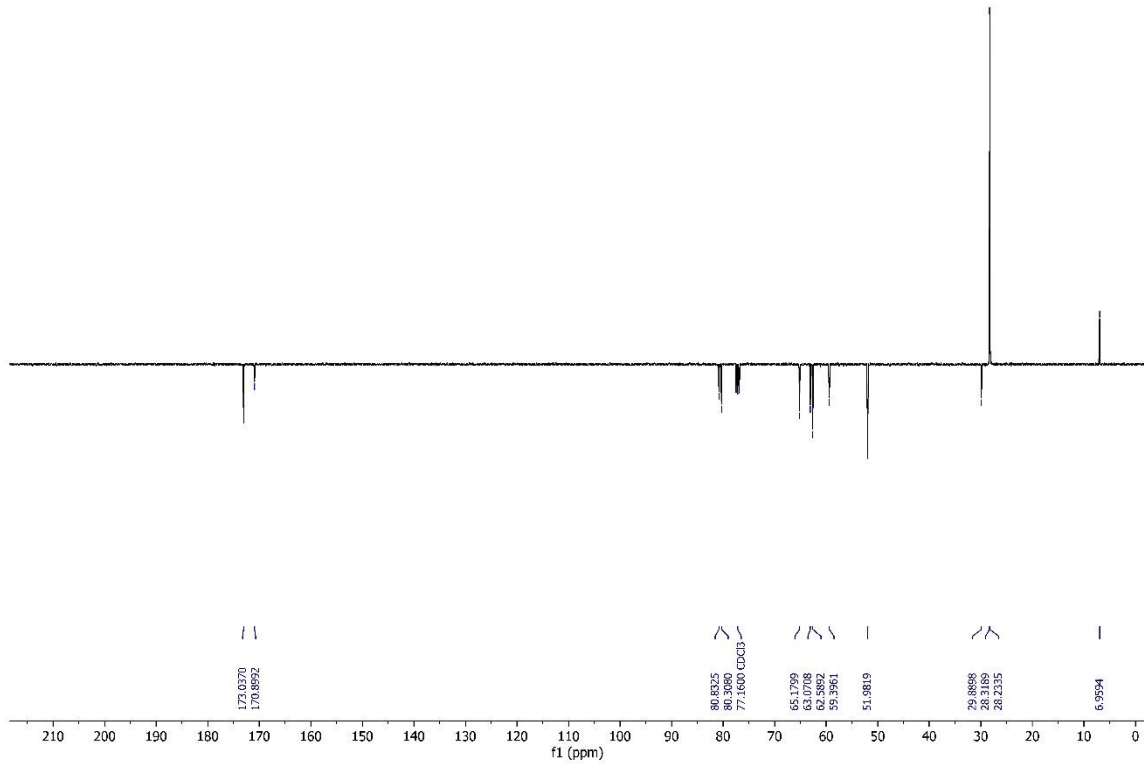
Figure S6. ^{13}C APT NMR spectrum of compound **4a**.
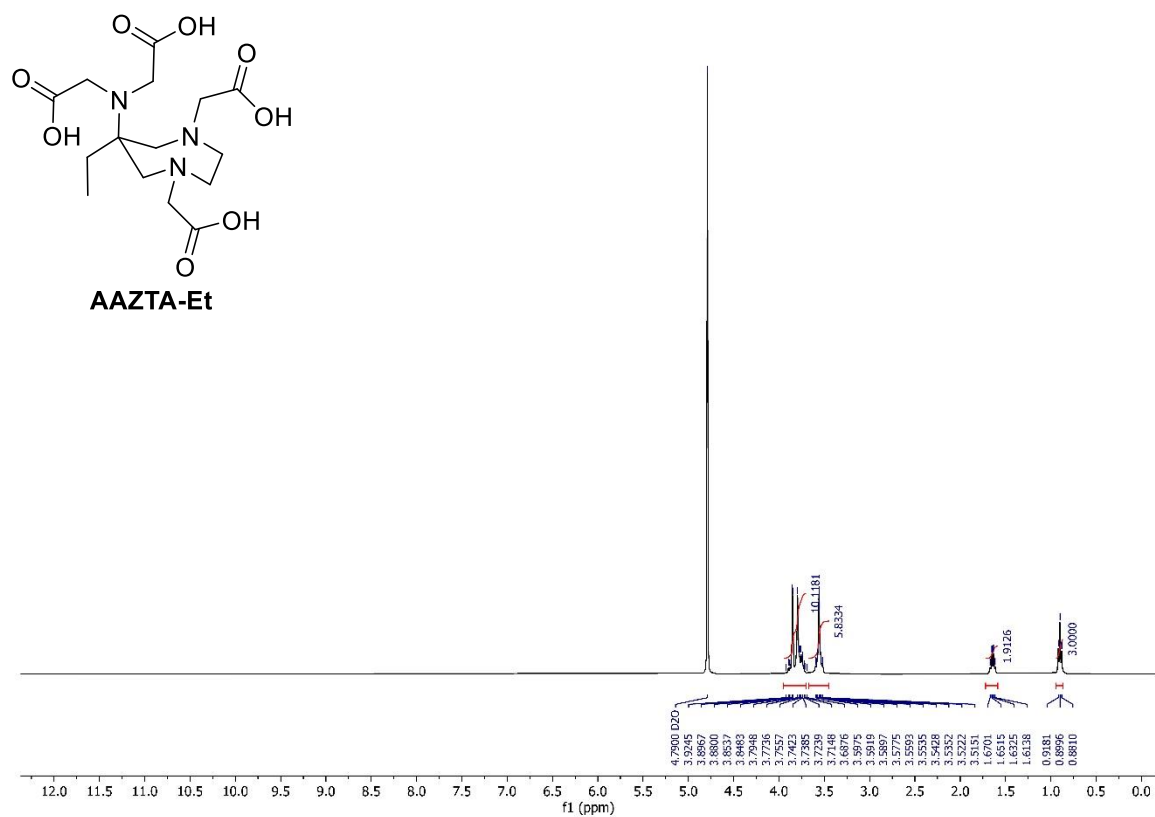
Figure S7. ^{1}H NMR spectrum of **AAZTA-Et**.
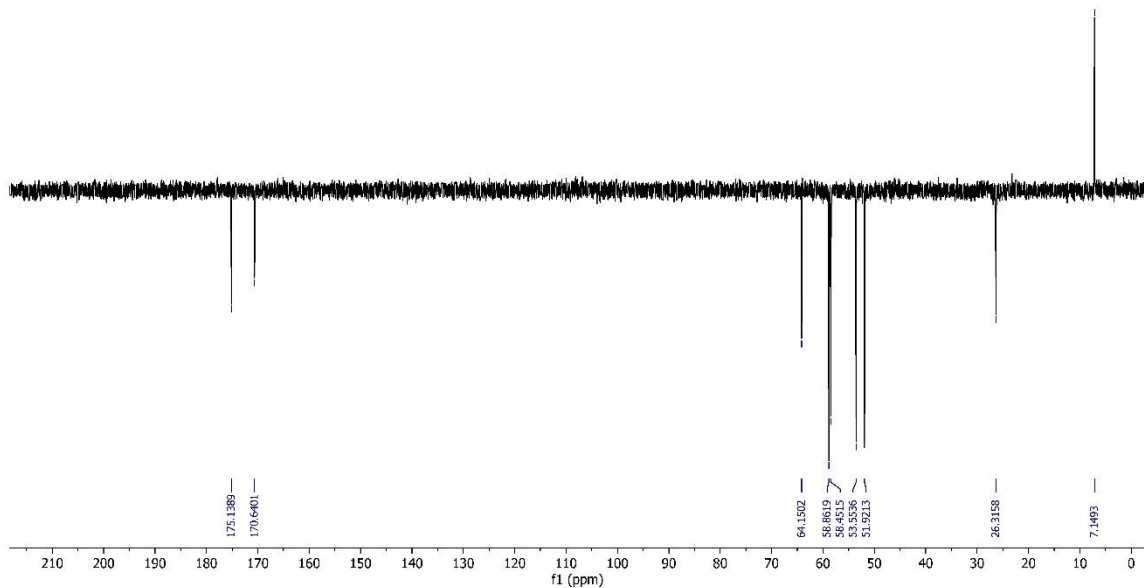
**Figure S8**. ^{13}C APT NMR spectrum of **AAZTA-Et**.
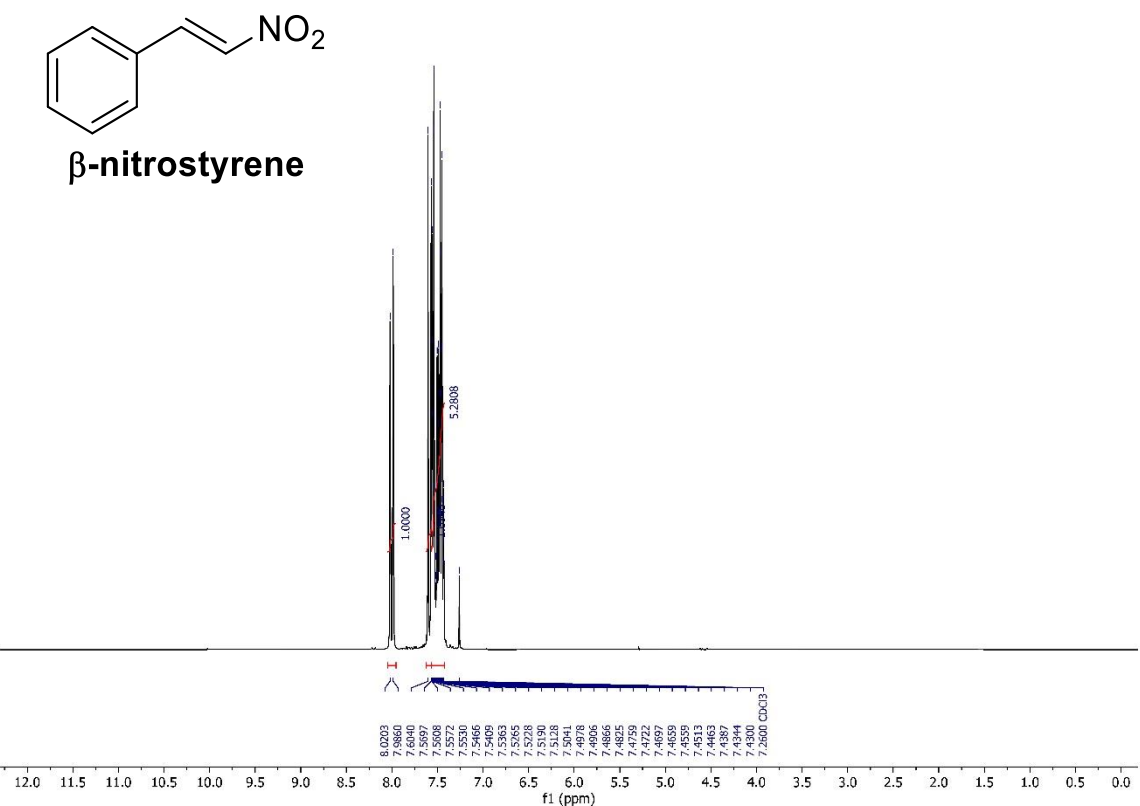
Figure S9. ^{1}H NMR spectrum of **β-nitrostyrene**.
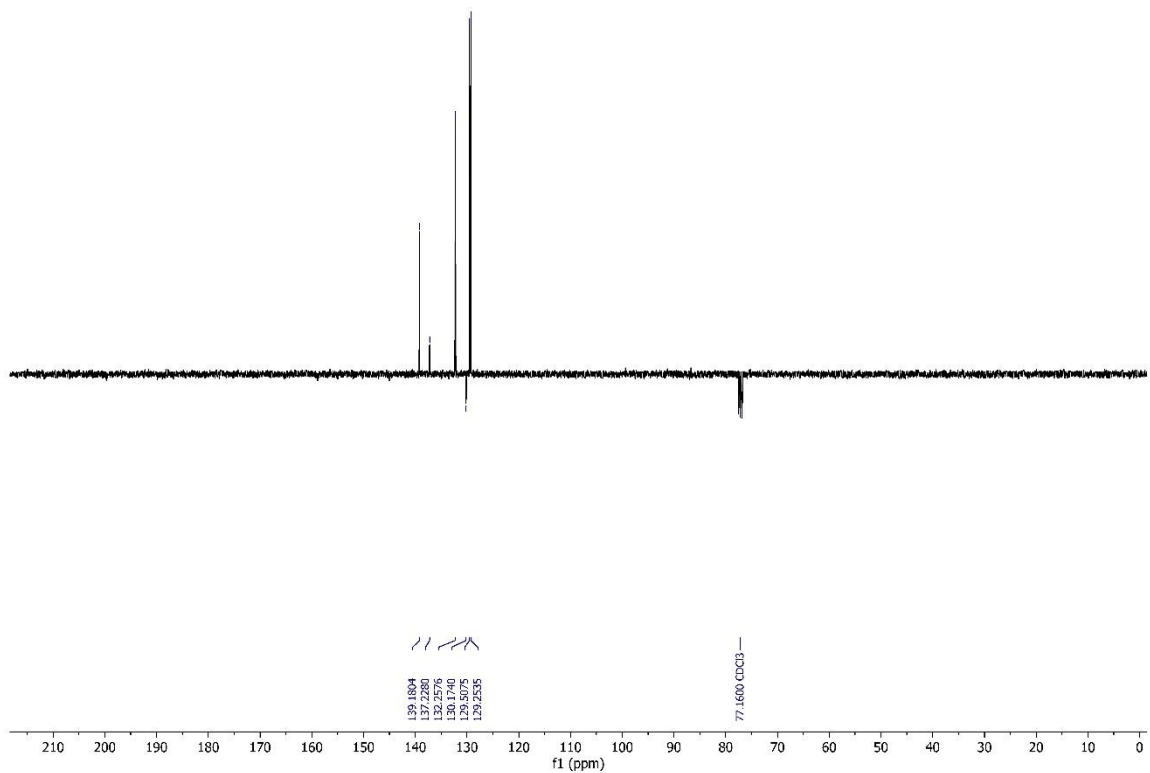
Figure S10. ^{13}C APT NMR spectrum of **β-nitrostyrene**.
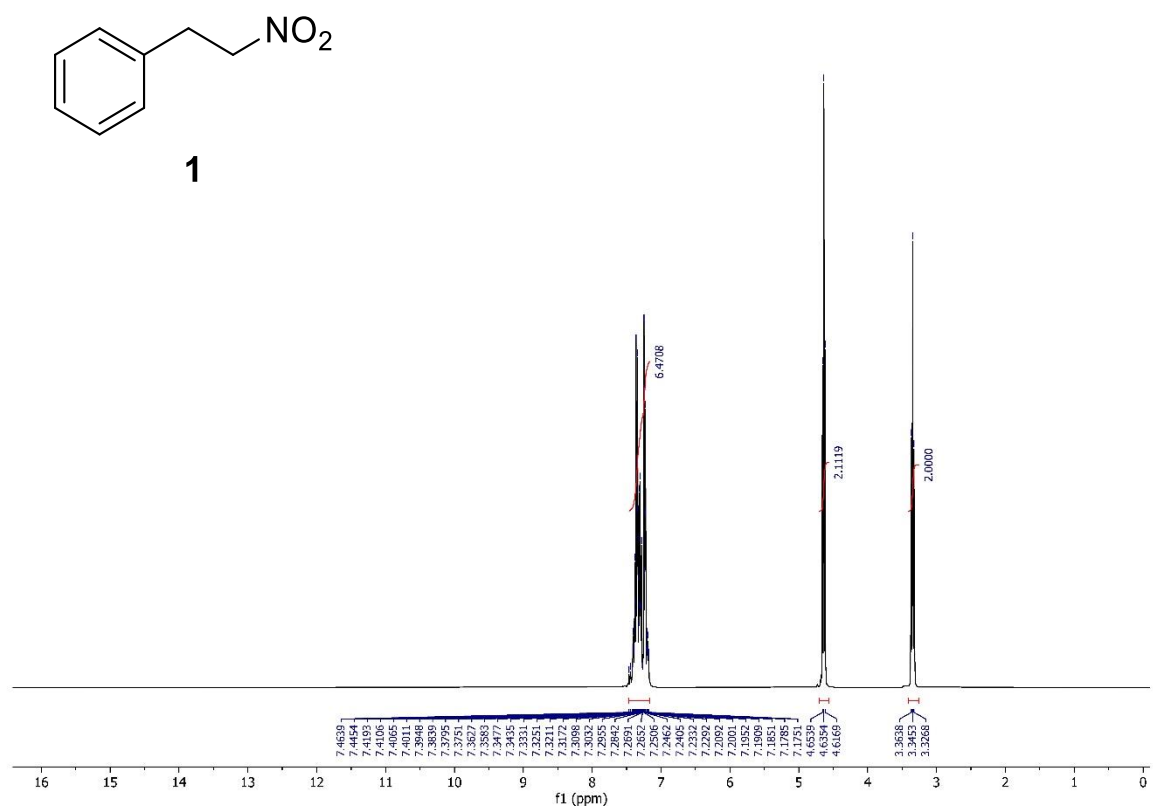
Figure S11. ^{1}H NMR spectrum of compound **1**.
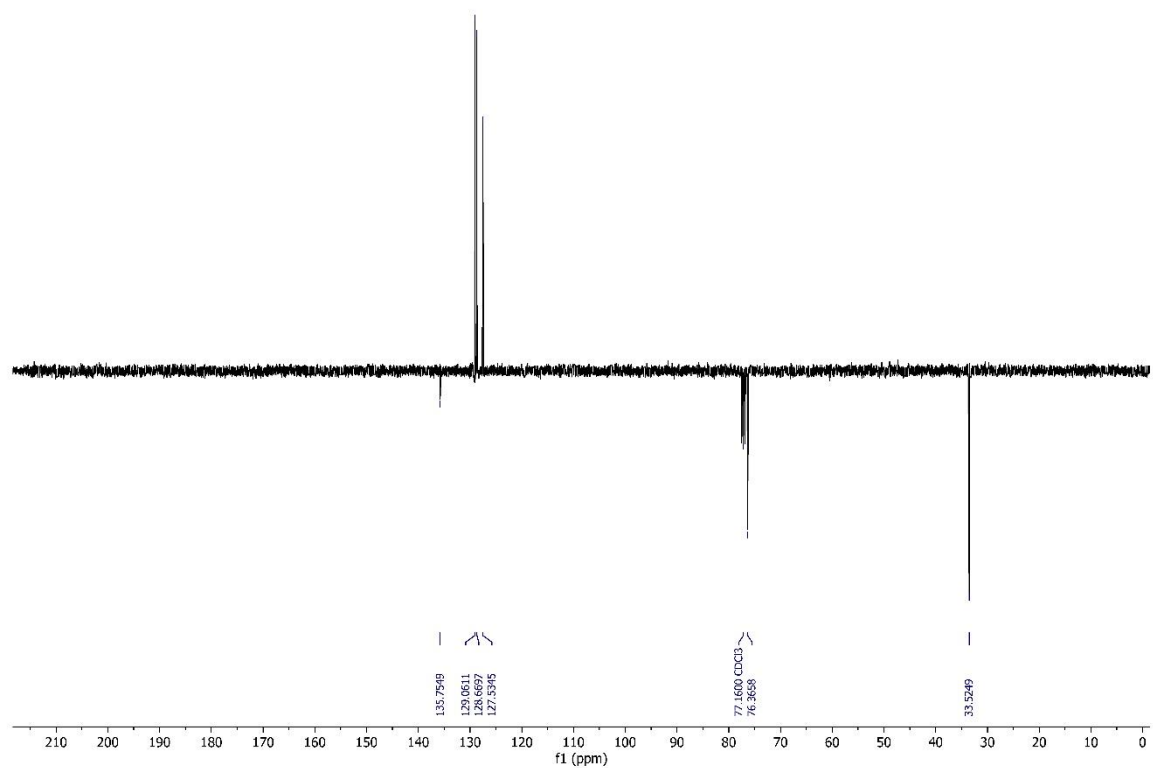
Figure S12. ^{13}C APT NMR spectrum of compound **1**.
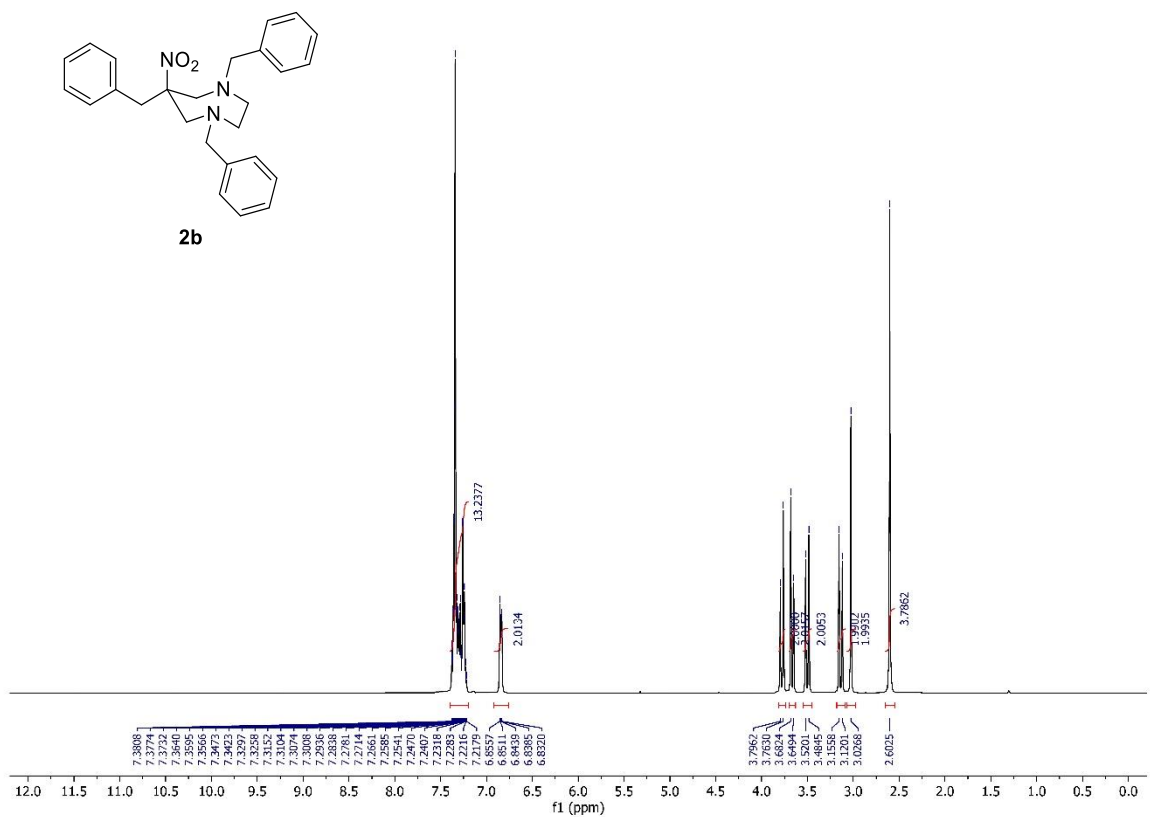
Figure S13. ^{1}H NMR spectrum of compound **2b**.
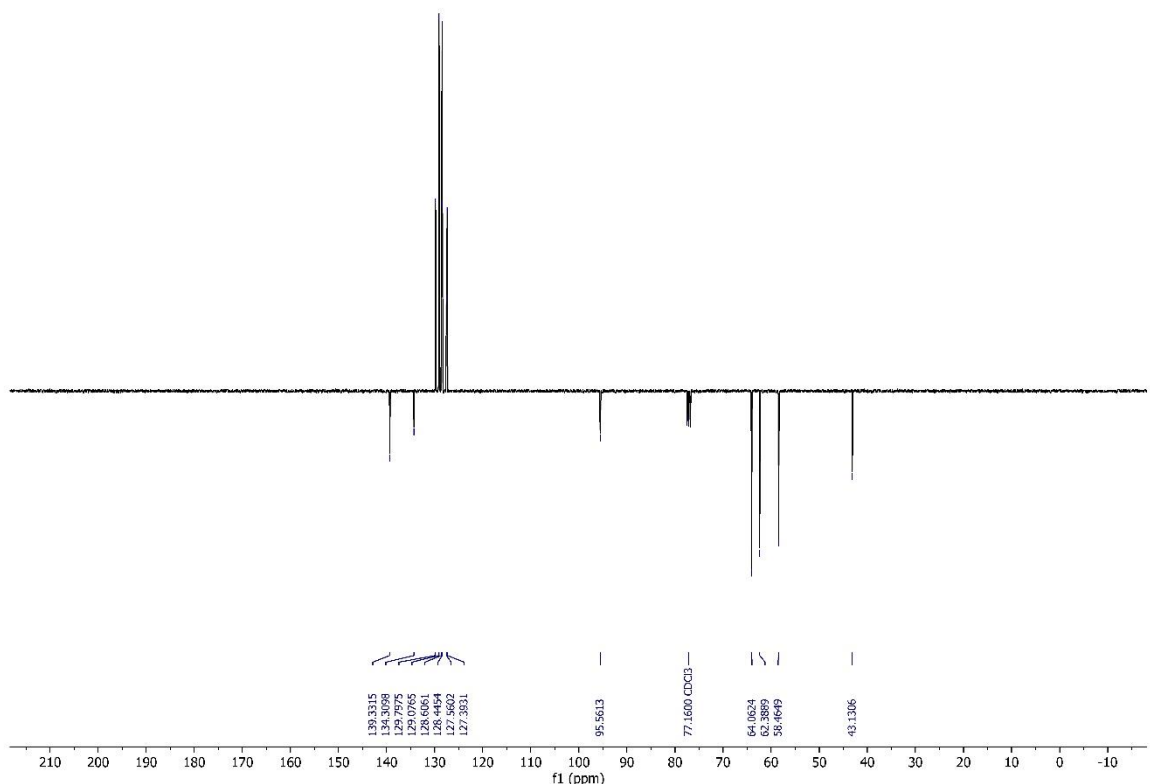
Figure S14. ^{13}C APT NMR spectrum of compound **2b**.
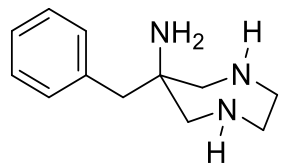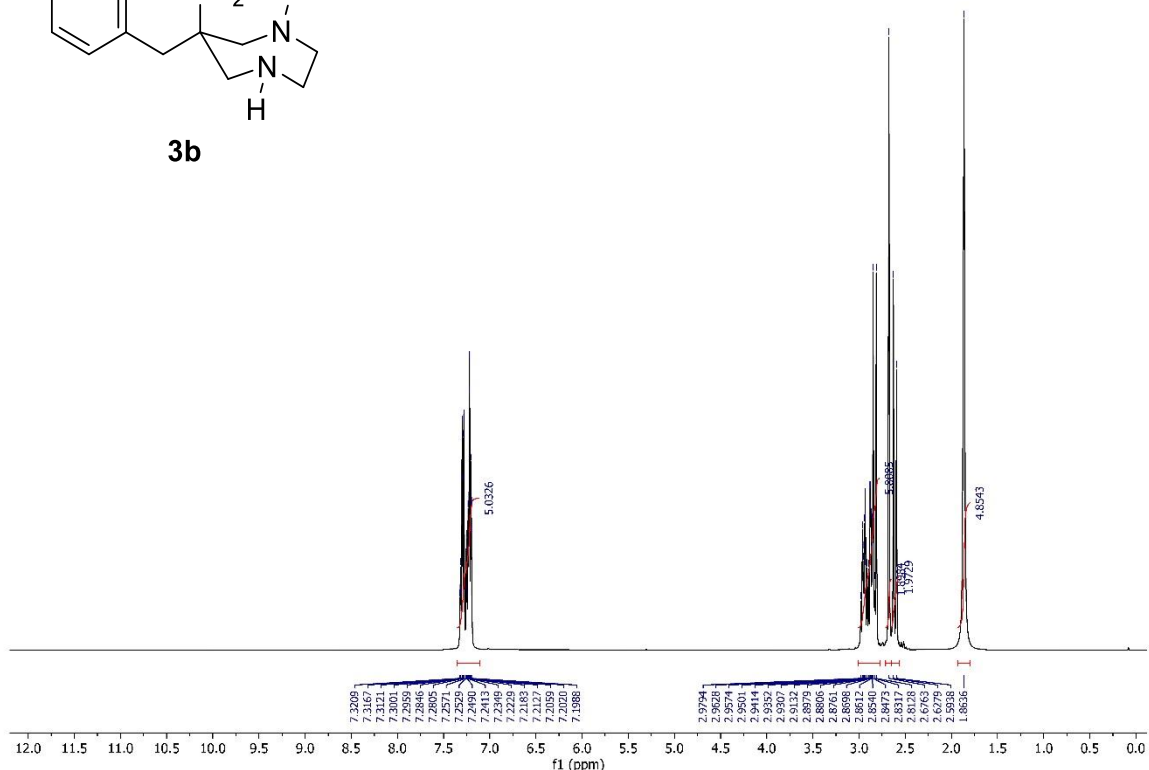
Figure S15. ^{1}H NMR spectrum of compound **3b**.
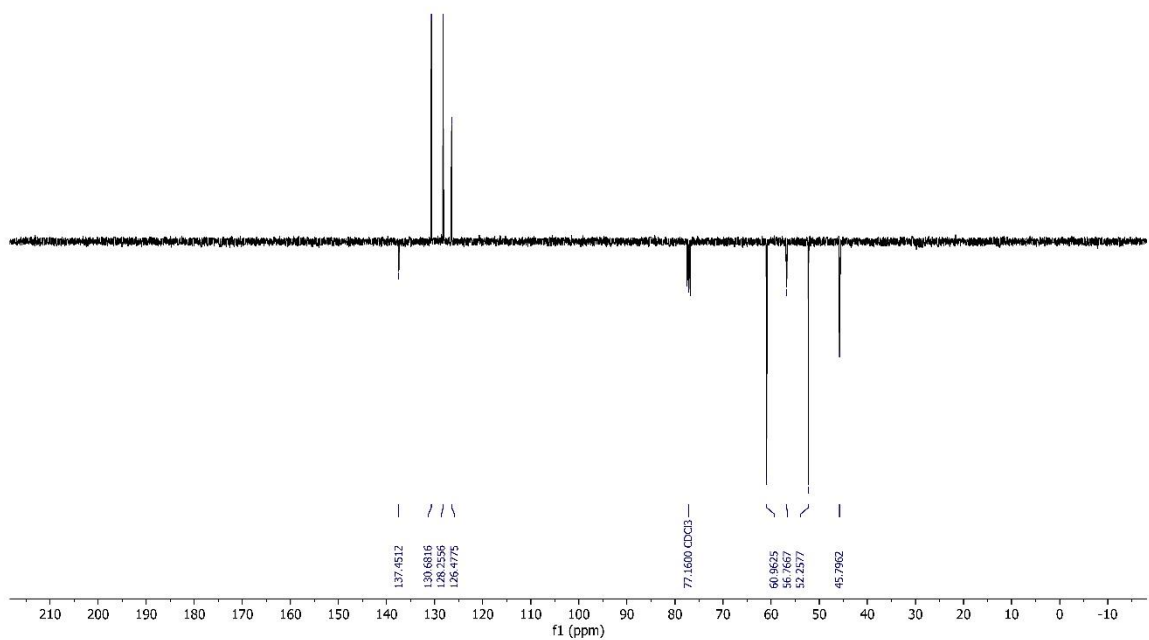
Figure S16. ^{13}C APT NMR spectrum of compound **3b**.
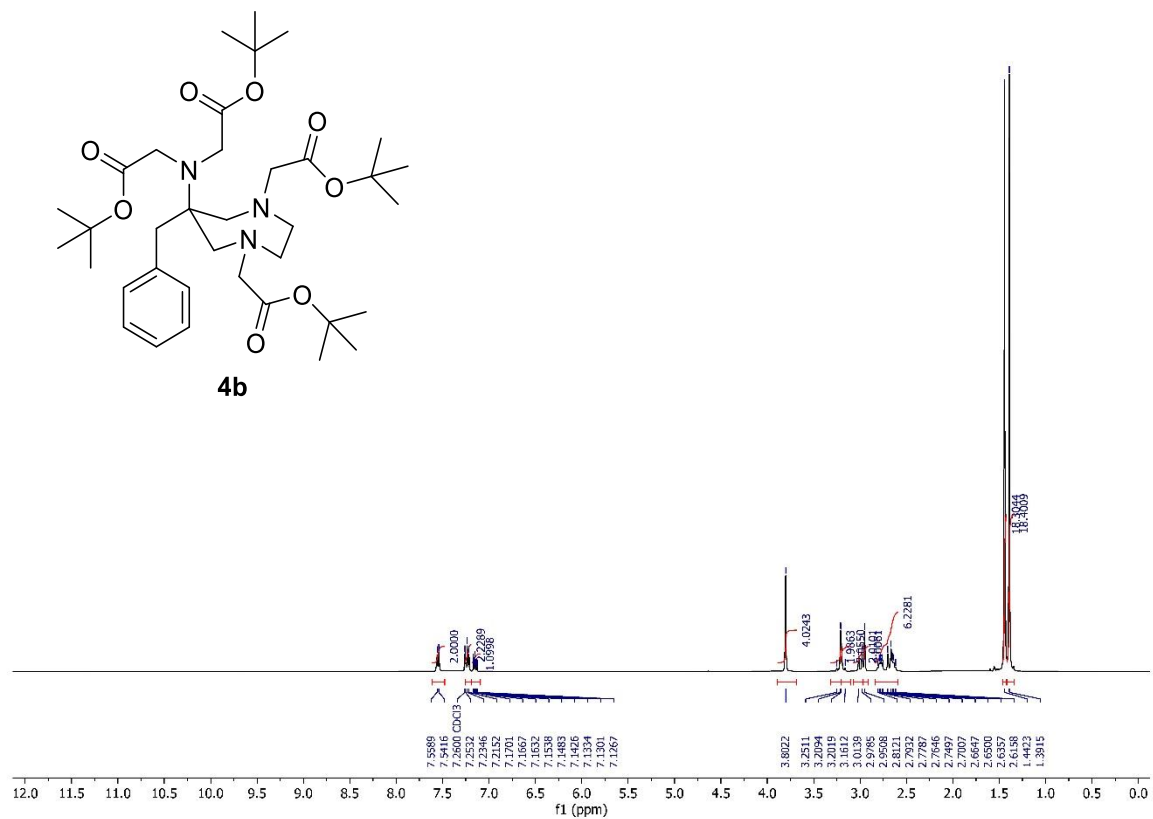
Figure S17. ^{1}H NMR spectrum of compound **4b**.
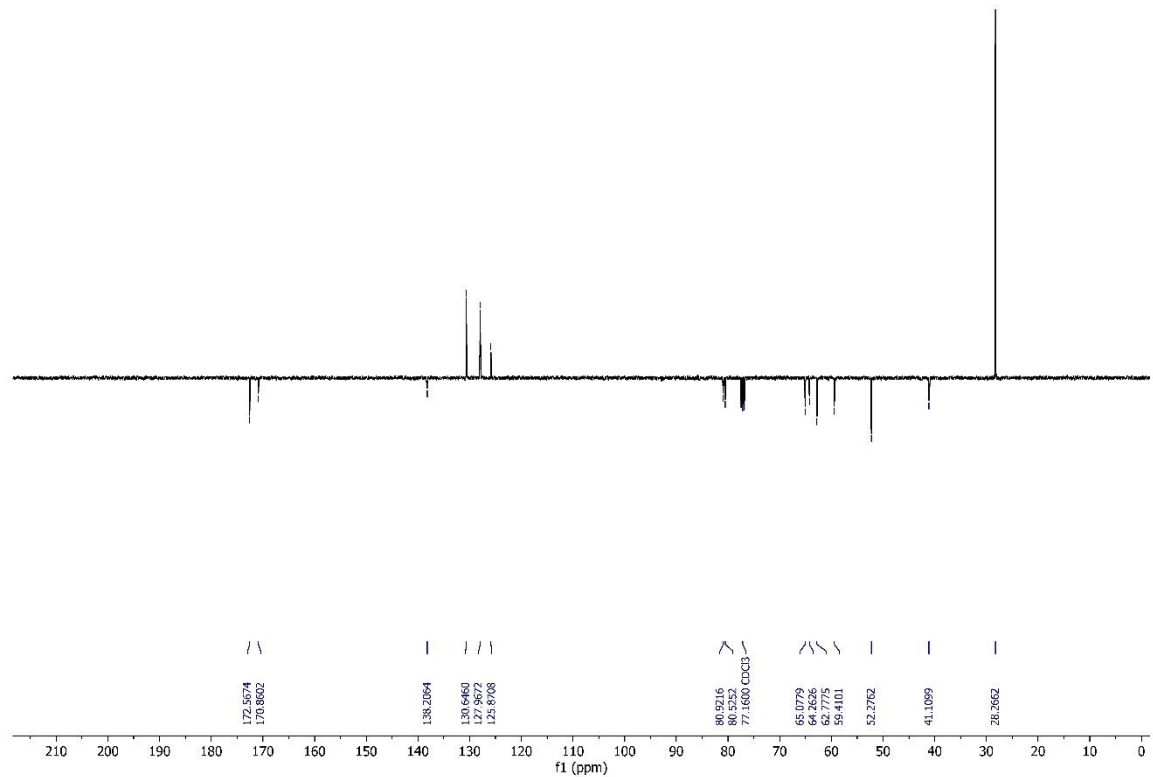
Figure S18. ^{13}C APT NMR spectrum of compound **4b**.
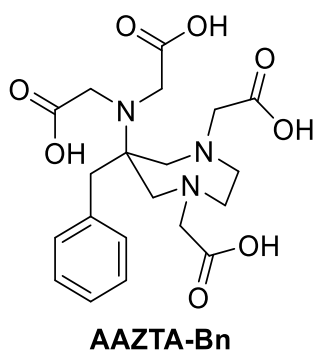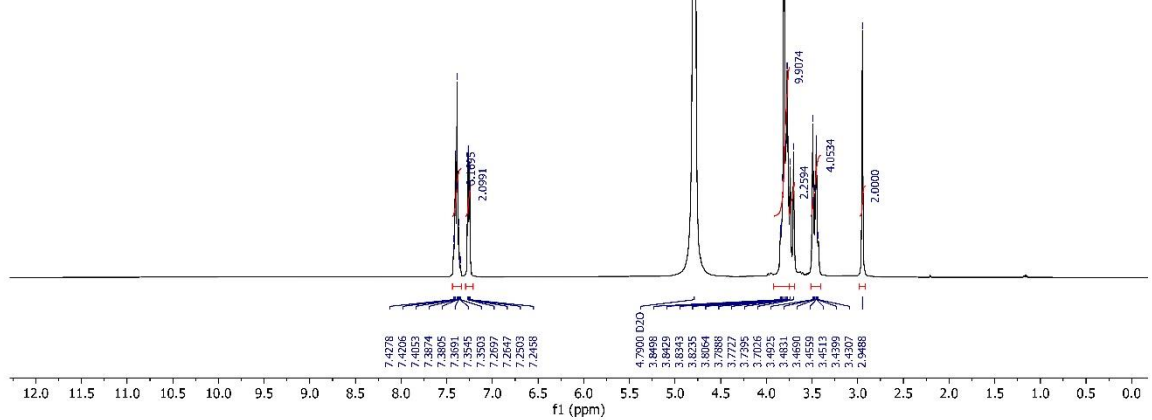
Figure S19. ^1H NMR spectrum of **AAZTA-Bn**.
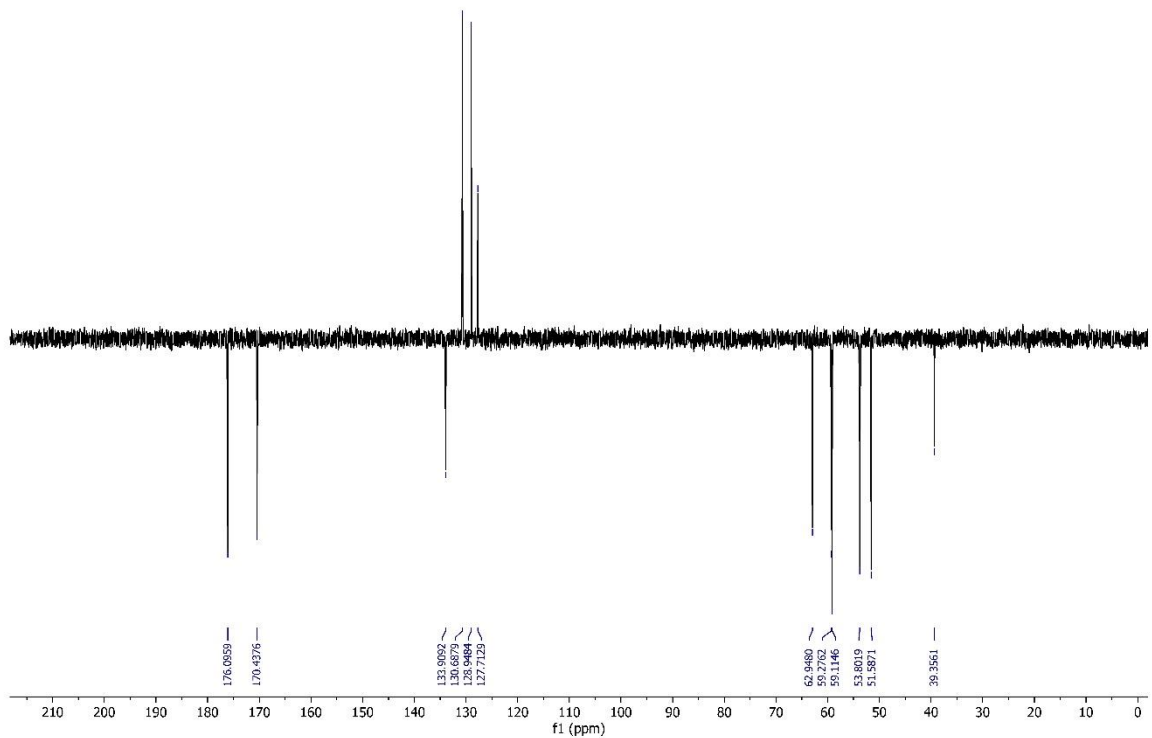
Figure S20. ^{13}C APT NMR spectrum of **AAZTA-Bn**.

Mass spectra
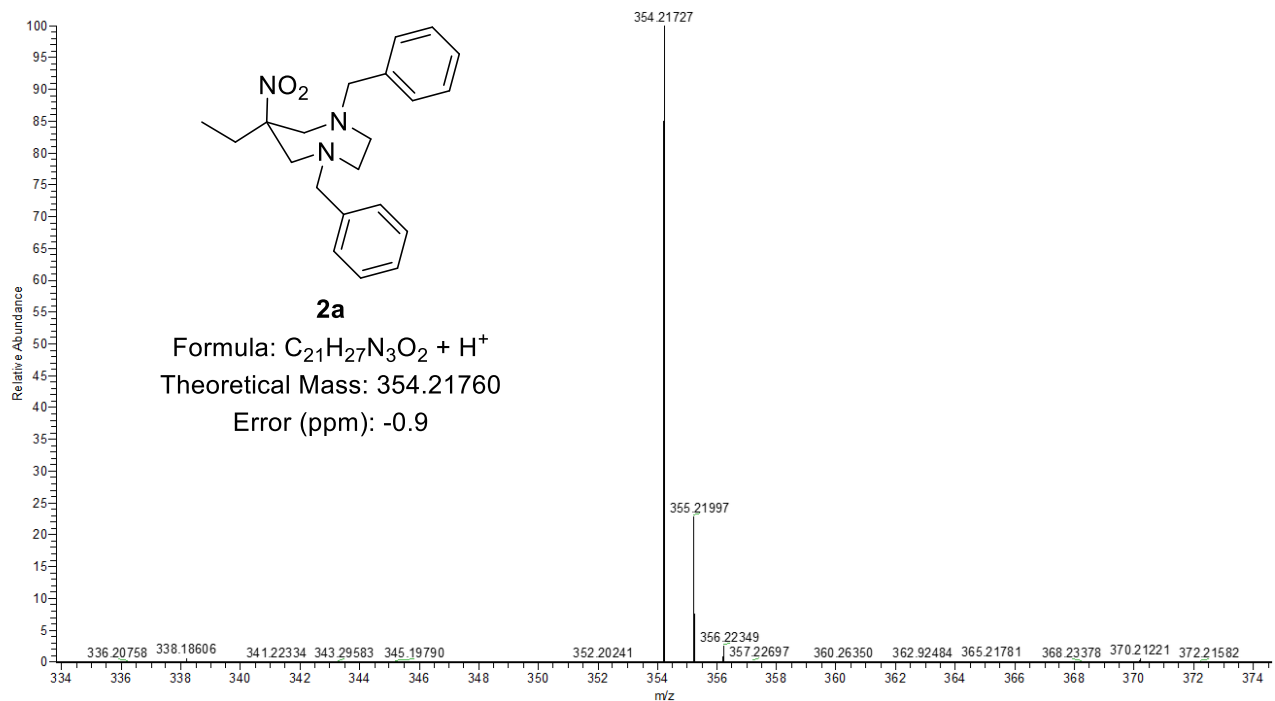
Figure S21. HRMS of compound **2a**.
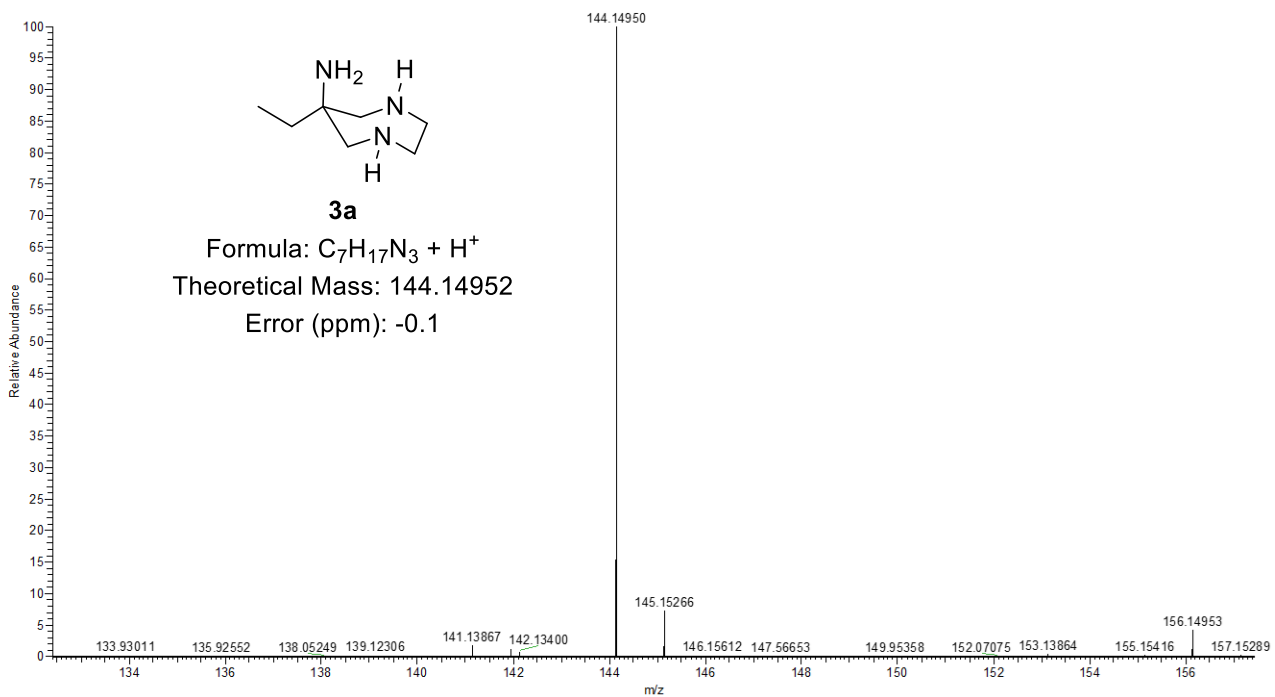
Figure S22. HRMS of compound **3a**.

4a

Formula: $C_{31}H_{57}N_3O_8 + H^+$
Theoretical Mass: 600.42184
Error (ppm): -0.9
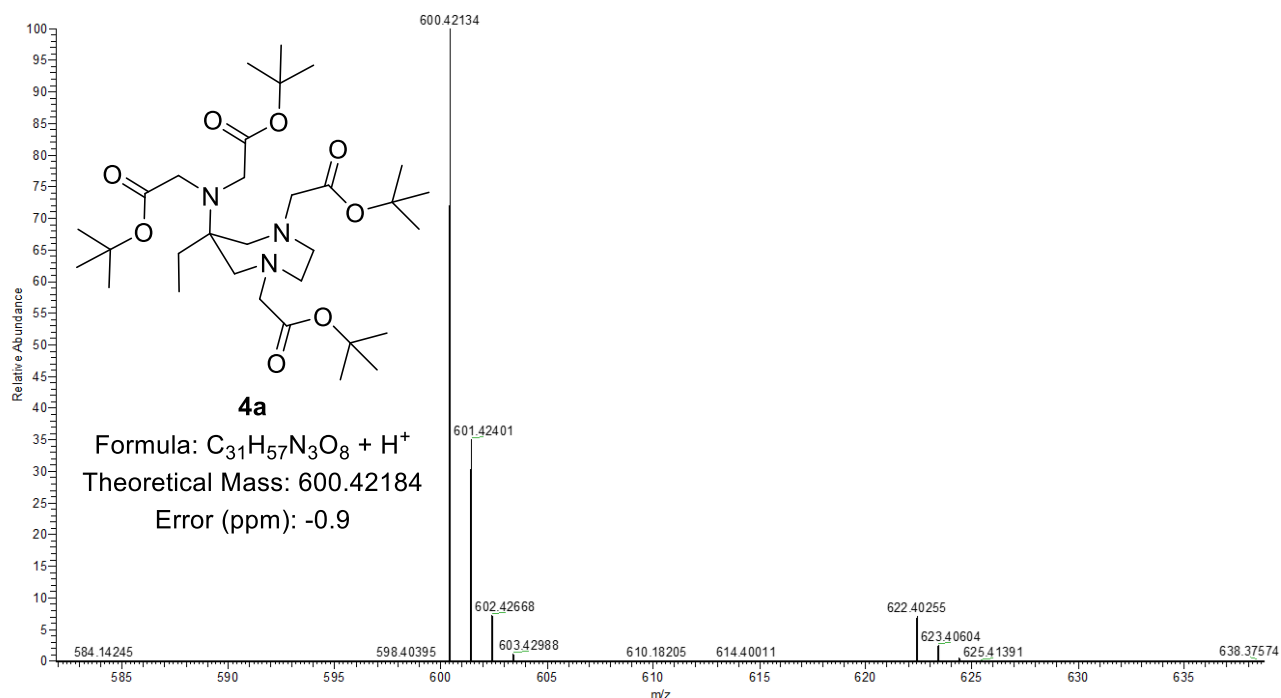
Figure S23. HRMS of compound **4a**.

AAZTA-Et

Formula: $C_{15}H_{25}N_3O_8 + H^+$
Theoretical Mass: 376.17144
Error (ppm): -1.0
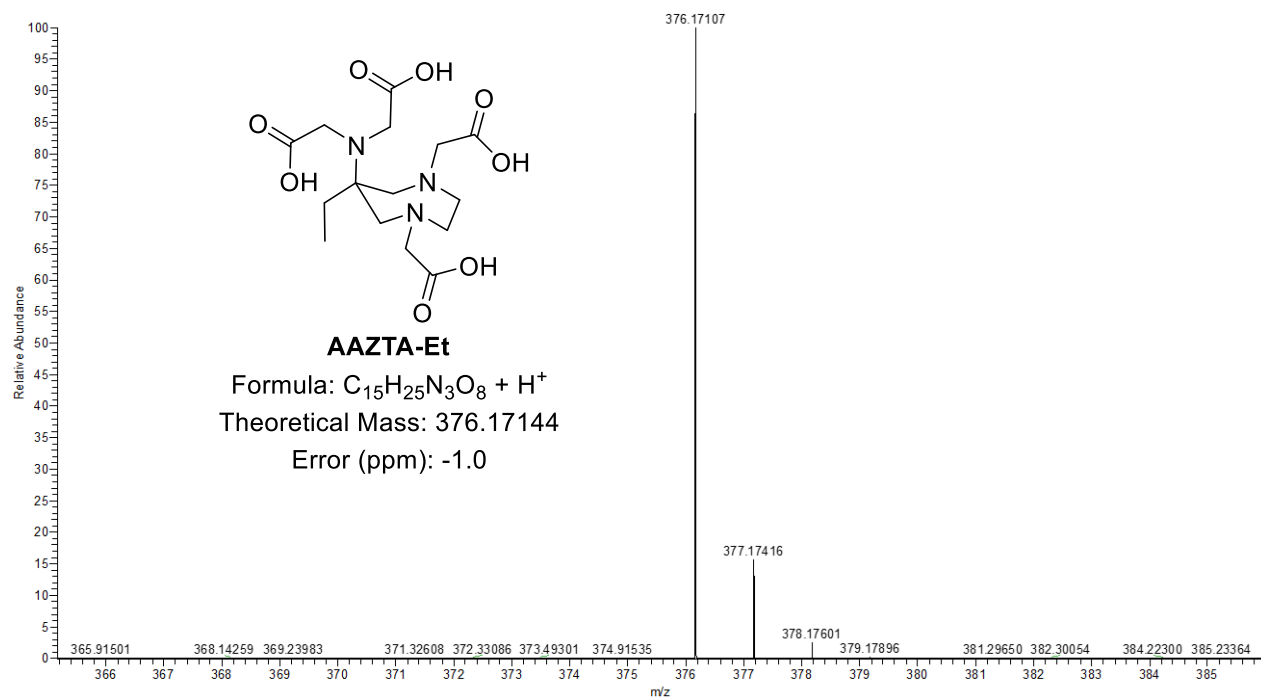
Figure S24. HRMS of **AAZTA-Et**.

2b
Formula: $C_{26}H_{29}N_3O_2 + H^+$
Theoretical Mass: 416.23325
Error (ppm): -1.4
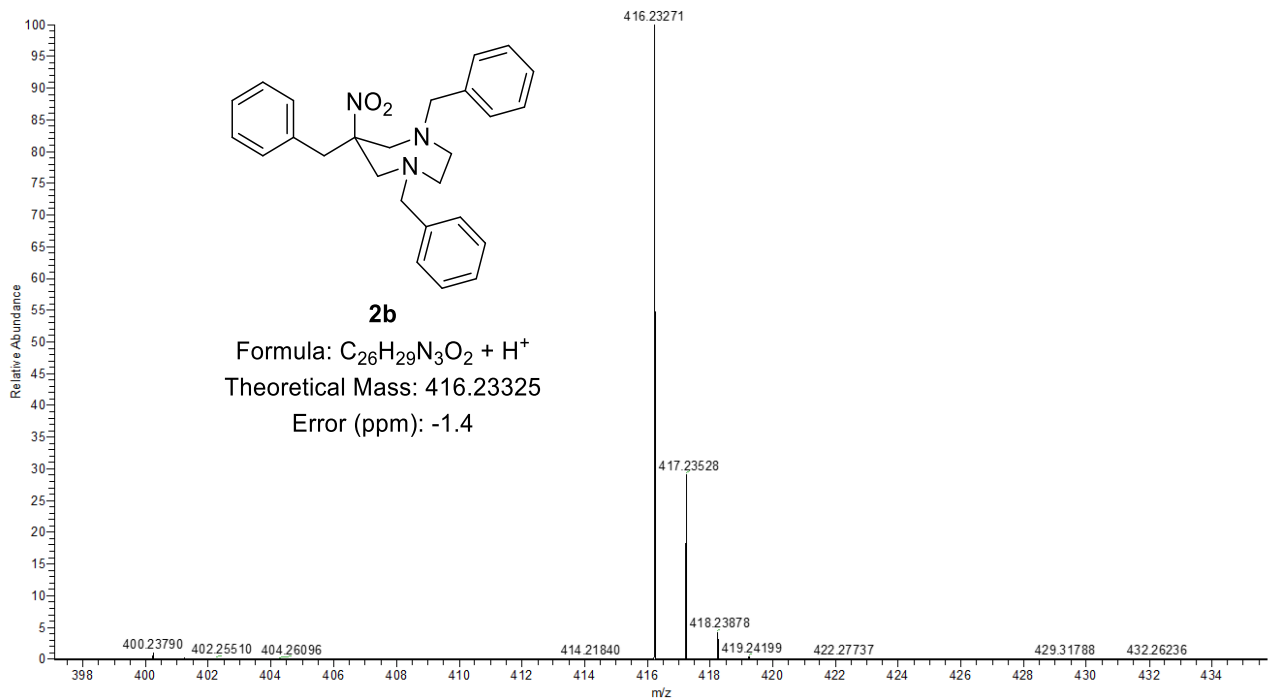
Figure S25. HRMS of compound **2b**.

3b
Formula: $C_{12}H_{19}N_3 + H^+$
Theoretical Mass: 206.16517
Error (ppm): -0.8
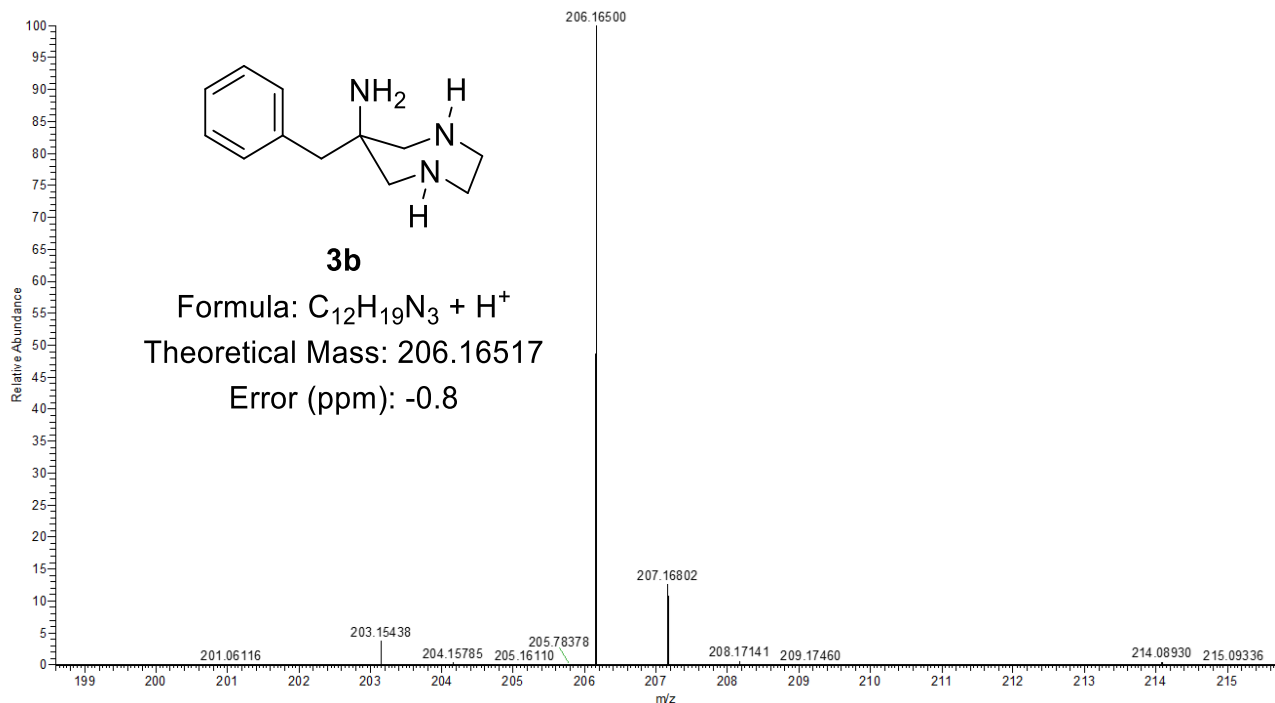
Figure S26. HRMS of compound **3b**.

4b

Formula: $C_{36}H_{59}N_3O_8 + H^+$
Theoretical Mass: 662.43749
Error (ppm): -1.2
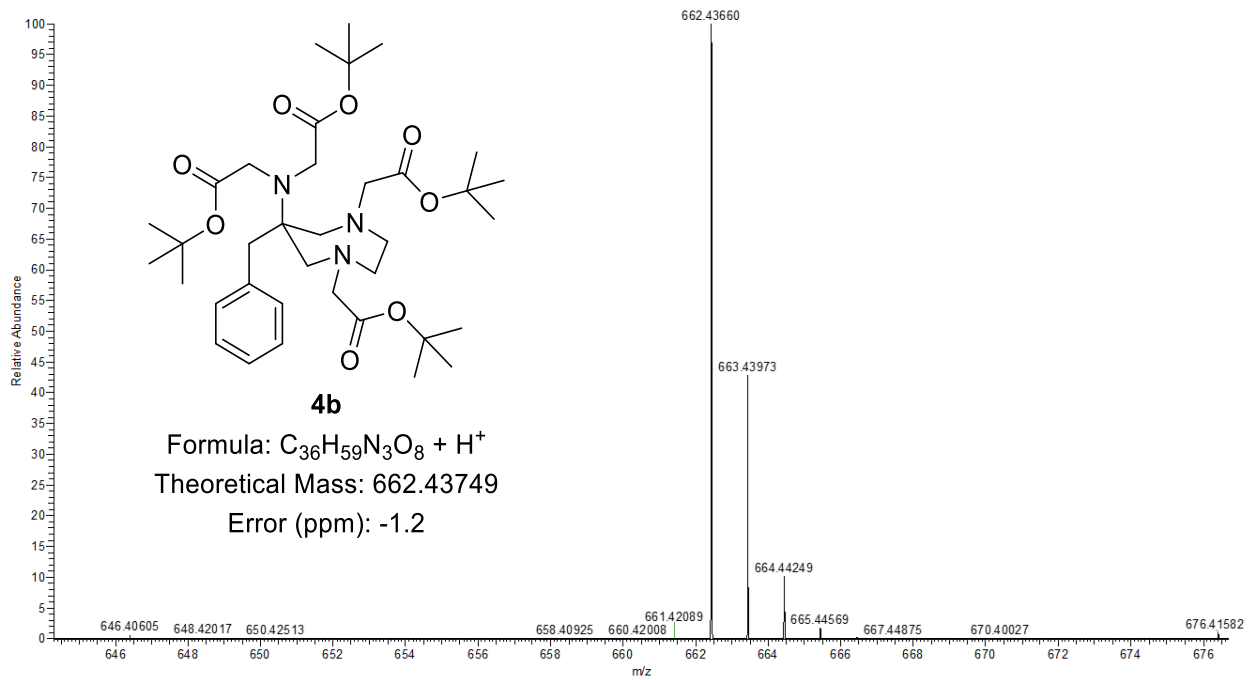
Figure S27. HRMS of compound **9**.

AAZTA-Bn

Formula: $C_{20}H_{27}O_8N_3 - H^+$
Theoretical Mass: 436.17254
Error (ppm): 0.5
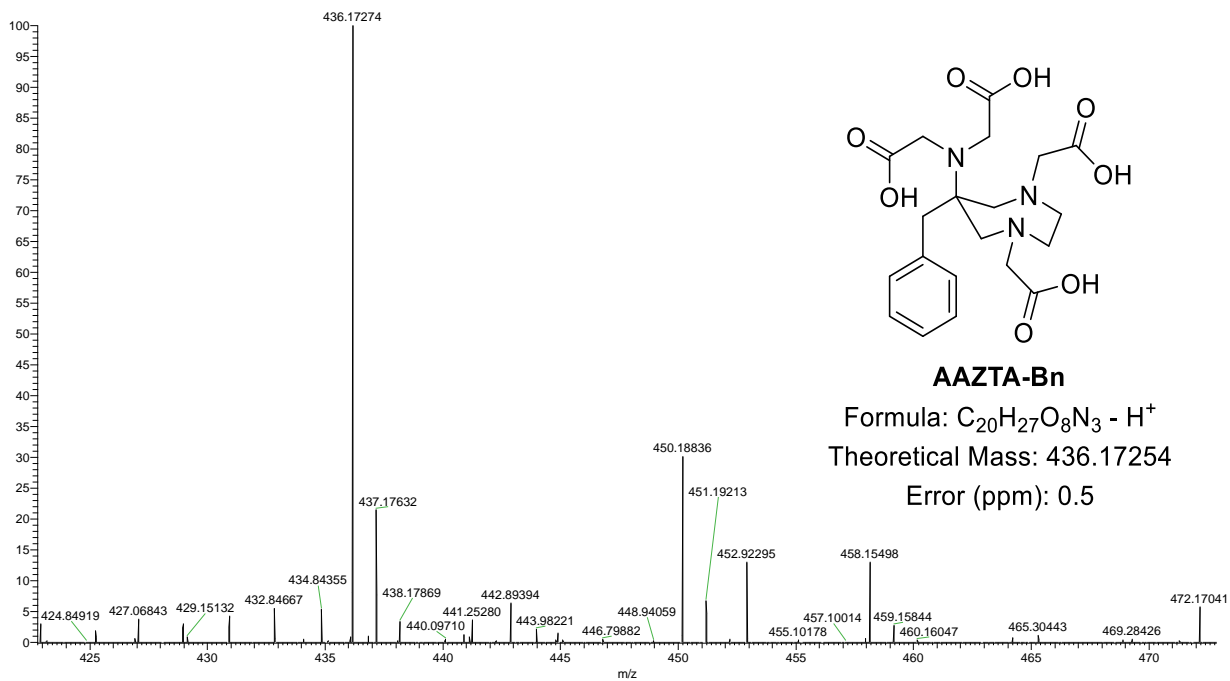
Figure S28. HRMS of **AAZTA-Bn**.

Equilibrium properties of AAZTA-Et and AAZTA-Bn ligands
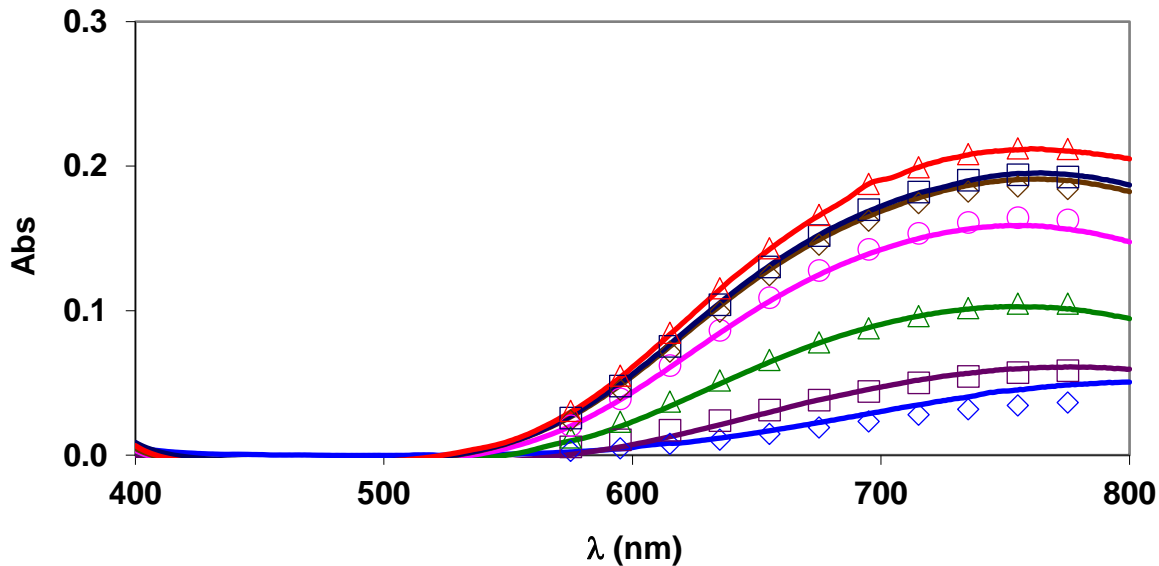
Figure S29. Absorption spectra of Cu^{2+}–AAZTA-Et systems. The solid lines and the open symbols represent the experimental and the calculated absorbance values, respectively. ($[Cu^{2+}]=[AAZTA-Et]=2.0$ mM, $[H^+]$ = **1.0 (◇)**, **0.60 (□)**, **0.31 (△)**, **0.10 (○)**, **0.04 (◇)**, **0.025 (□)** and **0.01 M (△)**, I=$[Na^+]+[H^+]$=0.15, $[H^+] \leq 0.15$ M, l=1 cm, 25°C)
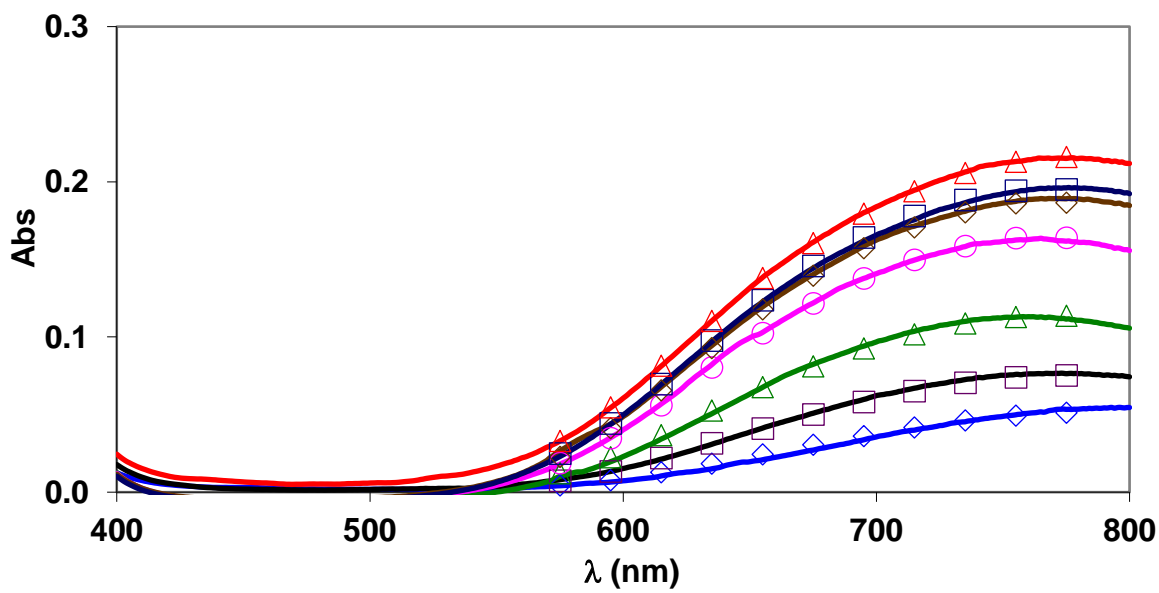
Figure S30. Absorption spectra of Cu^{2+}–AAZTA-Bn systems. The solid lines and the open symbols represent the experimental and the calculated absorbance values, respectively. ($[Cu^{2+}]=[AAZTA-Bn]=2.0$ mM, $[H^+]$ = **1.0 (◇)**, **0.60 (□)**, **0.31 (△)**, **0.10 (○)**, **0.04 (◇)**, **0.025 (□)** and **0.01 M (△)**, I=$[Na^+]+[H^+]$=0.15, $[H^+] \leq 0.15$ M, l=1 cm, 25°C)
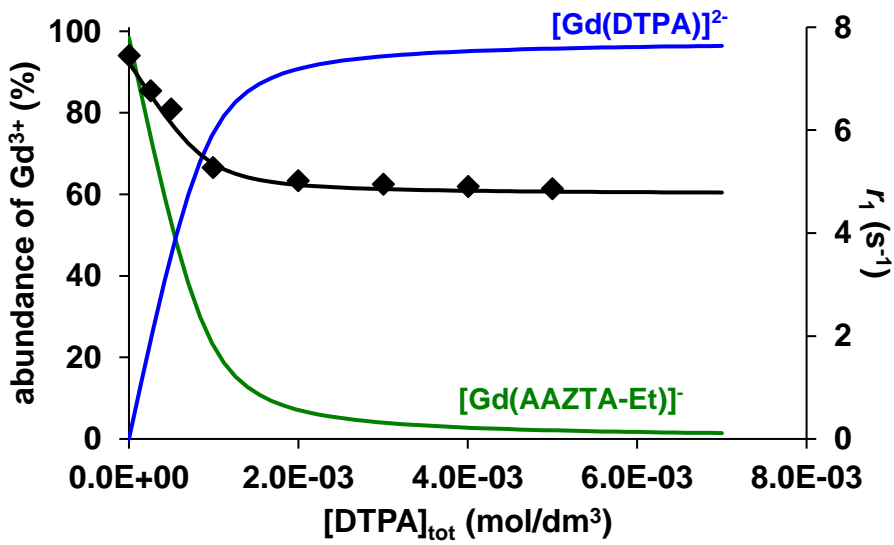
Figure S31. Relaxivity values of the Gd^{3+} - AAZTA-Et – DTPA systems at 21 MHz and pH=3.6 ([Gd^{3+}]=[AAZTA-Et]=1.0 mM, 25°C, 0.15 M NaCl)
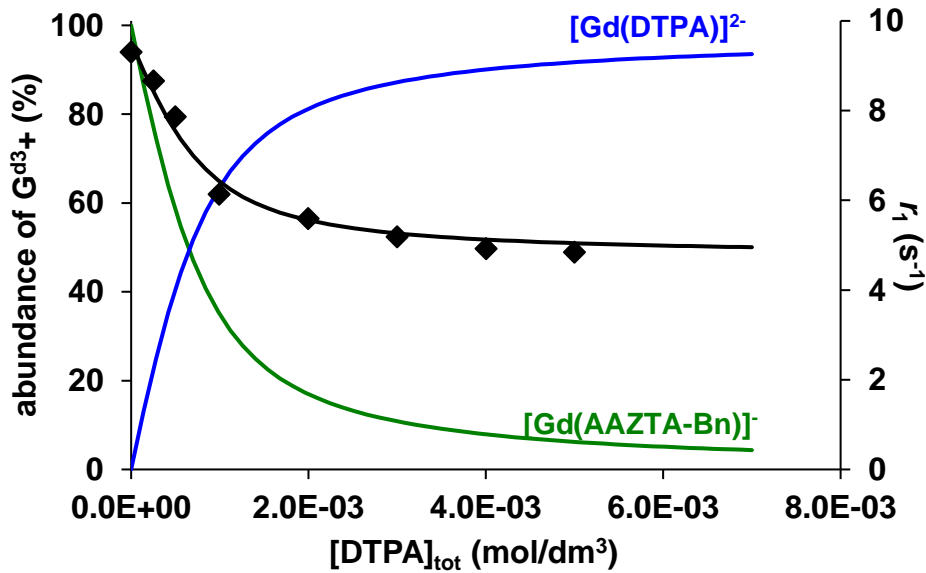
Figure S32. Relaxivity values of the Gd^{3+} - AAZTA-Bn – DTPA systems at 21 MHz and pH=3.6 ([Gd^{3+}]=[AAZTA-Bn]=1.0 mM, 25°C, 0.15 M NaCl)
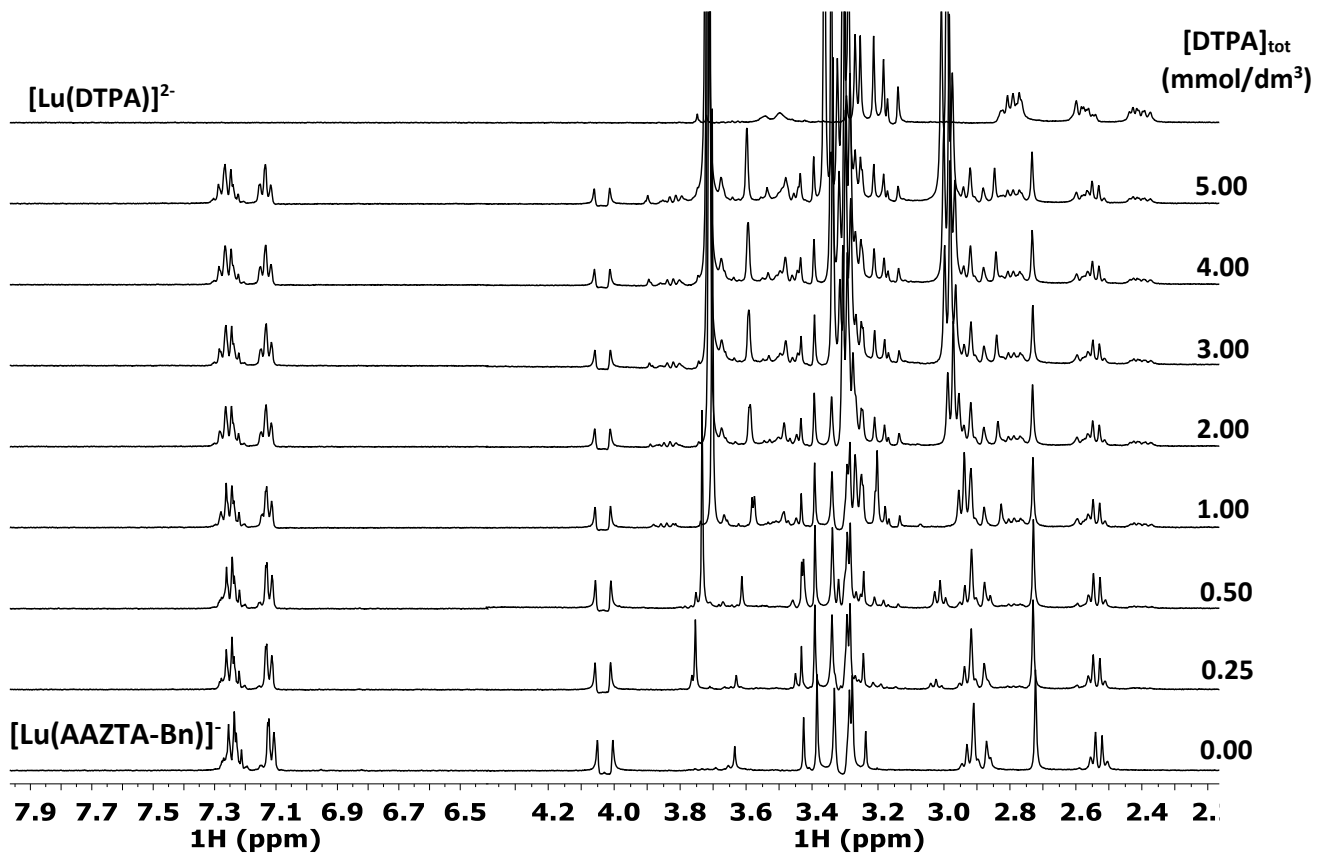
Figure S33. ^{1}H NMR spectra of the Lu^{3+} - AAZTA-Bn – DTPA systems at 400 MHz and pH=3.8 ([Lu^{3+}]=[AAZTA-Bn]=1.0 mM, 25°C, 0.15 M NaCl)
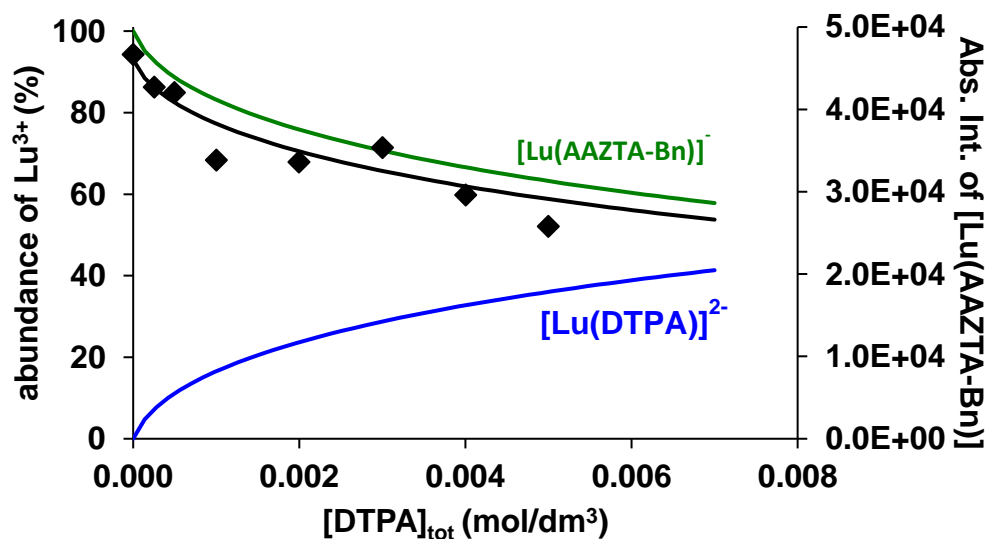
Figure S34. Abs. Int. values of the [Lu(AAZTA-Bn)]$^-$ in Lu^{3+} - AAZTA-Bn – DTPA systems at 400 MHz and pH=3.8 ([Lu^{3+}]=[AAZTA-Bn]=1.0 mM, 25°C, 0.15 M NaCl)

Kinetic inertness of [Gd(AAZTA-Et)]- and [Gd(AAZTA-Bn)]- complexes

The kinetic inertness of the [Gd(AAZTA-Et)]⁻ and [Gd(AAZTA-Bn)]⁻ complexes has been assessed by following the transmetalation reactions between the Gd^{3+} complexes and Cu^{2+} with spectrophotometry in the presence of Cu^{2+} excess (Eq. (S1)).

$$GdL \ + \ Cu^{2+} \ \rightleftharpoons \ CuL \ + \ Gd^{3+} \qquad\qquad (S1)$$

The rates of the transmetalation reactions have been investigated at different concentrations of Cu^{2+} in the pH range 2.8 – 4.5 ([GdL]=1.0 mM, [Cu^{2+}]=10 – 40 mM, 0.15 M NaCl, 25°C). In the presence of the 10 – 40 fold Cu^{2+} excess the transmetalation can be regarded as a pseudo-first-order process and the rate of reactions can be expressed with the Eq. (S2).

$$-\frac{d[GdL]_t}{dt} = k_d[GdL]_t$$
$$(S2)$$

where k_d is a pseudo-first-order rate constant and [GdL]$_t$ is the concentration of GdL species at the time t, respectively. The pseudo-first-order rate constants (k_d) for the transmetalation reactions of [Gd(AAZTA-Et)]⁻ and [Gd(AAZTA-Bn)]⁻ with Cu^{2+} are plotted as a function of pH and [H⁺] in Figures S35 and S36, respectively. The kinetic data presented in Figures S35 and S36 indicates that the k_d values characterizing the transmetalation reaction of [Gd(AAZTA-Et)]⁻ and [Gd(AAZTA-Bn)]⁻ with Cu^{2+} increase with increase of the [H⁺] and decrease with the increase of [Cu^{2+}] at pH<4.0. The transmetalation reactions of Gd^{3+} complexes with AAZTA derivatives take place by the slow rate determining dissociation of the Gd^{3+} complexes followed by a fast reaction between the free ligand and the exchanging metal ions.[1–3] The dependence of k_d on the [H⁺] can be expressed as a first-order function of [H⁺] which indicates that the exchange can take place by proton-independent (k_0, Eq. (S3)) and proton assisted ($k_{Gd(HL)}$, Eq. (S5)) pathways. The proton assisted dissociations of Gd^{3+} complexes can be explained by the equilibrium formation of a protonated Gd(HL) species (Eq. (S4)), which can slowly dissociate to the free Gd^{3+} ion and the ligand.

$$GdL \ \xrightarrow{k_0} \ Gd^{3+} \ + \ L \qquad\qquad (S3)$$

$$GdL \ + \ H^+ \ \overset{K_{Gd(HL)}}{\rightleftharpoons} \ Gd(HL) \qquad\qquad (S4)$$

$$K_{Gd(HL)} = \frac{[Gd(HL)]}{[GdL][H^+]}$$

$$Gd(HL) \ \xrightarrow{k_{Gd(HL)}} \ Gd^{3+} \ + \ HL \qquad\qquad (S5)$$
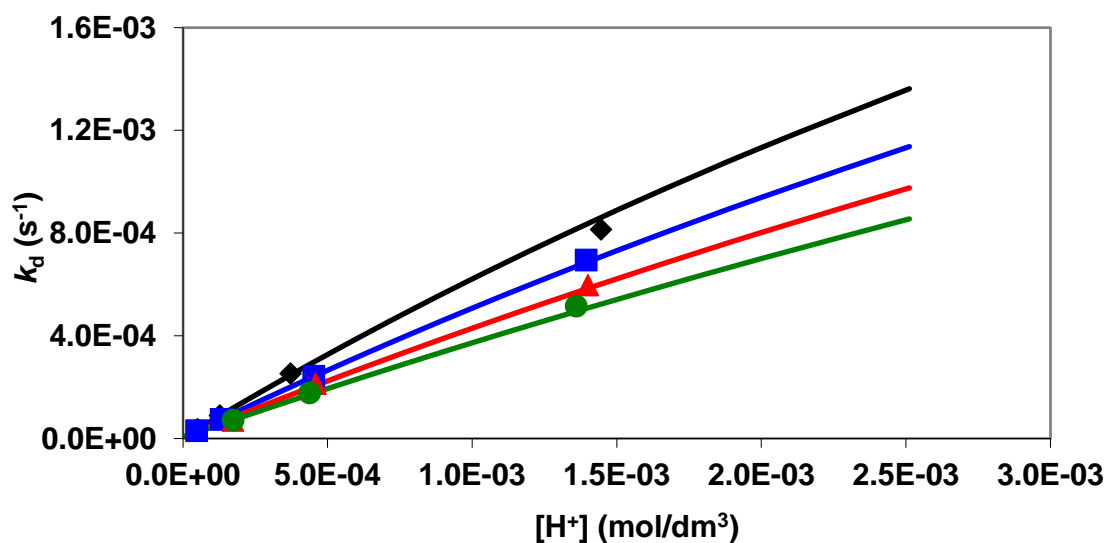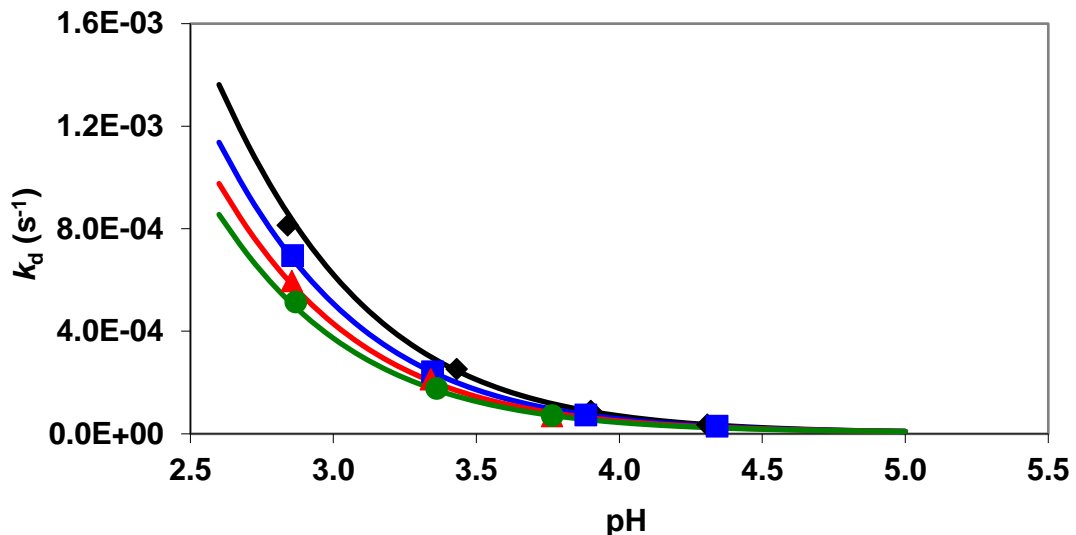
Figure S35. Pseudo-first order rate constants (k_d) characterize the transmetalation reactions of [Gd(AAZTA-Et)]$^-$ with Cu^{2+} as a function of pH and [H$^+$] ([GdL] = 0.5 mM, [Cu^{2+}] = 10 (◆), 20 (■), 30 (▲) and 40 mM (●) (10 mM DMP and NMP, 0.15 M NaCl, 25 °C).
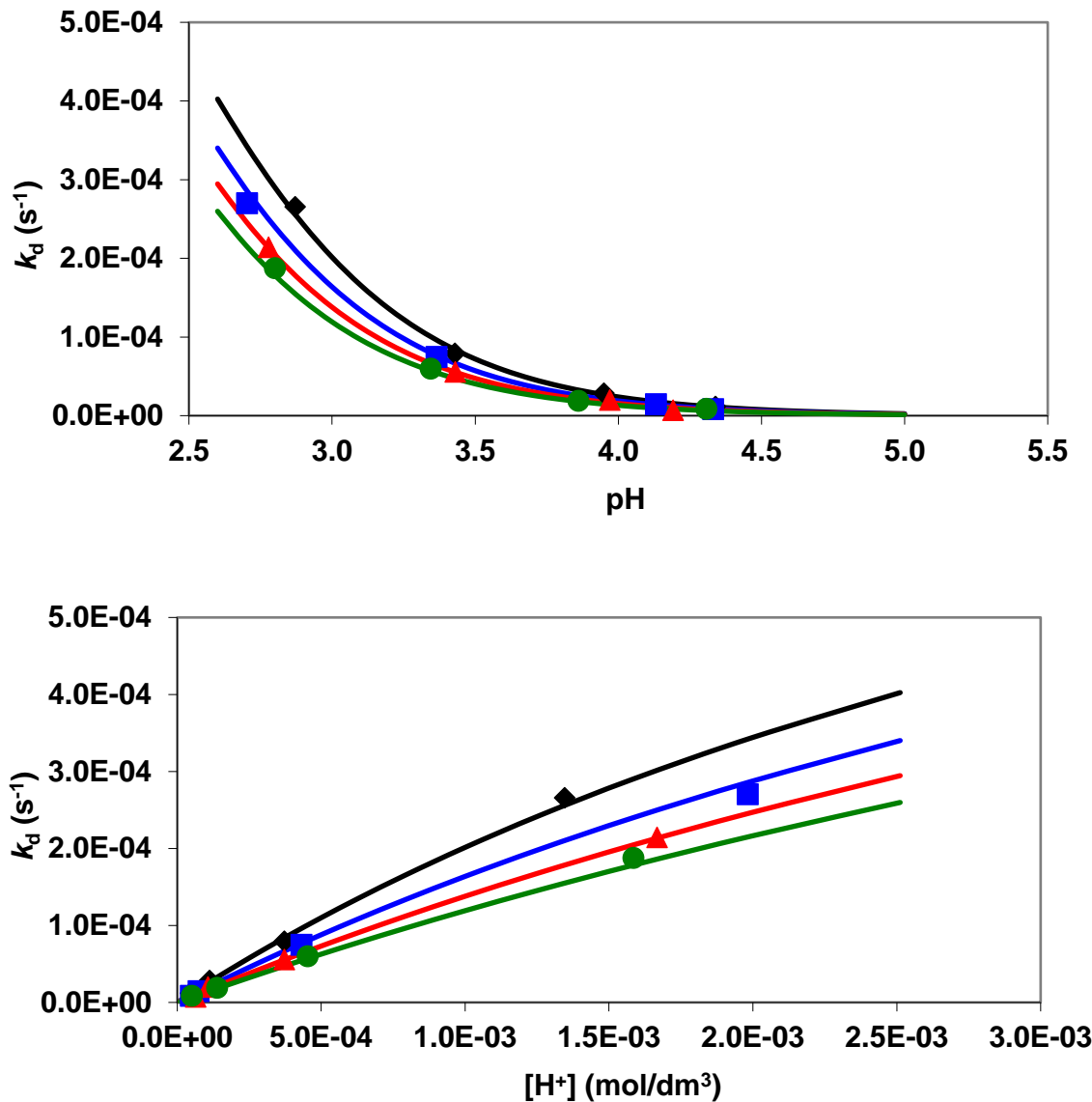
Figure S36. Pseudo-first order rate constants (k_d) characterize the transmetalation reactions of [Gd(AAZTA-Bn)]⁻ with Cu^{2+} as a function of pH and [H⁺] ([GdL] = 0.5 mM, [Cu^{2+}] = 10 (◆), 20 (■), 30 (▲) and 40 mM (●)) (10 mM DMP and NMP, 0.15 M NaCl, 25 °C).

The trend observed in the k_d values of [Gd(AAZTA-Et)]⁻ and [Gd(AAZTA-Bn)]⁻ (Figures S35 and S36) is unusual since the k_d values decrease with the increase of [Cu^{2+}] at higher H⁺ concentrations. At lower [H⁺], the k_d rate constants slightly increase with the increase of [Cu^{2+}] Similar behaviours have been identified for the transmetalation reactions of [Gd(AAZTA)]⁻, [Gd(AAZTA-C2-COO⁻)]²⁻ and [Ln(DTPA)]²⁻ complexes with Cu^{2+}, Zn^{2+} and Eu^{3+} ions.[1,3,4] It has been evidenced that the presence of large exchanging metal ion excess results in the formation of hetero-dinuclear [Ln(DTPA)]Eu⁺ and [Lu(AAZTA)]Cu⁺ complex, which was detected by ¹H-NMR spectroscopy.[1,5] According to the kinetic data, the formation of hetero-dinuclear Gd(L)Cu intermediate might take place ($K_{Gd(L)Cu}$, Eq. (S6)) in which the functional groups of the AAZTA-Et or AAZTA-Bn ligands are slowly transferred from the Gd^{3+} to the exchanging Cu^{2+} ion ($k_{Gd(L)Cu}$, Eq. (S7)) promoting the dissociation of the Gd^{3+} ion and the formation of the corresponding CuL complex.

$$\text{GdL} \; + \; \text{Cu}^{2+} \; \rightleftharpoons \; [\text{Gd(L)Cu}] \qquad (S6)$$
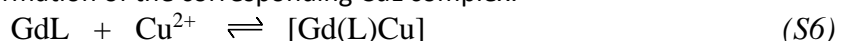
$$K_{Gd(L)Cu} = \frac{[\text{Gd(L)Cu}]}{[\text{GdL}][\text{Cu}^{2+}]}$$

$$[Gd(L)Cu] \xrightarrow{k_{Gd(L)Cu}} Gd^{3+} + CuL \qquad (S7)$$

The decrease of the k_d values in the presence of large Cu^{2+} excess (Figures S35 and S36) can be explained by the equilibrium formation of the hetero-dinuclear Gd(L)Cu intermediate (Eq. (S6)) resulting in the lower concentration of the more reactive protonated Gd(HL) species and the smaller contribution of the proton-assisted pathway to the overall dissociation rate of the [Gd(AAZTA-Et)]⁻ and [Gd(AAZTA-Bn)]⁻ complexes.

By taking into account all the possible pathways, the rate of the transmetalation of [Gd(AAZTA-Et)]⁻ and [Gd(AAZTA-Bn)]⁻ complexes can be expressed by Eq. (S8), where the [Gd(HL)] and [Gd(L)Cu] are the concentrations of the monoprotonated and the heterodinuclear complexes, respectively.

$$-\frac{[GdL]_t}{dt} = k_0[GdL] + k_{Gd(HL)}[Gd(HL)] + k_{Gd(L)Cu}[Gd(L)Cu] \qquad (S8)$$

Considering total concentration of the complex ([GdL]$_t$=[GdL]+[Gd(HL)]+[Gd(L)Cu]), the equation defining the protonation constant of the GdL species (Eq. (S4)), the stability constant of the hetero-dinuclear Gd(L)Cu complex (Eq. (S6)) and Eq. (S8), the pseudo-first-order rate constant can be expressed as follows:

$$k_d = \frac{k_0 + k_1[H^+] + k_3^{Cu}[Cu^{2+}]}{1 + K_{Gd(HL)}[H^+] + K_{Gd(L)Cu}[Cu^{2+}]} \qquad (S9)$$

where k_0, k_1=$k_{Gd(HL)} \times K_{Gd(HL)}$ and k_3^{Cu}= $k_{Gd(L)Cu} \times K_{Gd(L)Cu}$ are the rate constants characterising the spontaneous, proton- and metal-assisted dissociation of the [Gd(AAZTA-Et)]⁻ and [Gd(AAZTA-Bn)]⁻ complexes, respectively. The rate and equilibrium constants that characterise the transmetalation reaction of [Gd(AAZTA-Et)]⁻ and [Gd(AAZTA-Bn)]⁻ were calculated by fitting the k_d values presented in Figures S35 and S36 to Eq. (S9).

References

1. Baranyai, Z.; Uggeri, F.; Giovenzana, G.B.; Bényei, A.; Brücher, E.; Aime, S. Equilibrium and Kinetic Properties of the Lanthanoids(III) and Various Divalent Metal Complexes of the Heptadentate Ligand AAZTA. *Chem. Eur. J.* **2009**, *15*, 1696–1705, doi:10.1002/chem.200801803.
2. Baranyai, Z.; Pálinkás, Z.; Uggeri, F.; Maiocchi, A.; Aime, S.; Brücher, E. Dissociation Kinetics of Open-Chain and Macrocyclic Gadolinium(III)-Aminopolycarboxylate Complexes Related to Magnetic Resonance Imaging: Catalytic Effect of Endogenous Ligands. *Chem. Eur. J.* **2012**, *18*, 16426–16435, doi:10.1002/chem.201202930.
3. Kock, F.V.C.; Forgács, A.; Guidolin, N.; Stefania, R.; Vágner, A.; Gianolio, E.; Aime, S.; Baranyai, Z. [Gd(AAZTA)]⁻ Derivatives with n-Alkyl Acid Side Chains Show Improved Properties for Their Application as MRI Contrast Agents. *Chemistry – A European Journal* **2021**, *27*, 1849–1859, doi:10.1002/chem.202004479.
4. Sarka, L.; Burai, L.; Brücher, E. The Rates of the Exchange Reactions between [Gd(DTPA)]²⁻ and the Endogenous Ions Cu²⁺ and Zn²⁺: A Kinetic Model for the Prediction of the In Vivo Stability of [Gd(DTPA)]²⁻, Used as a Contrast Agent in Magnetic Resonance Imaging. *Chem. Eur. J.* **2000**, *6*, 719–724, doi:10.1002/(SICI)1521-3765(20000218)6:4<719::AID-CHEM719>3.0.CO;2-2.
5. Brücher, E.; Laurenczy, G. Aminopolycarboxylates of Rare Earths—VIII: Kinetic Study of Exchange Reactions between Eu³⁺ Ions and Lanthanide(III) Diethylenetriaminepentaacetate Complexes. *Journal of Inorganic and Nuclear Chemistry* **1981**, *43*, 2089–2096, doi:10.1016/0022-1902(81)80555-6.